Title

Residual Stress From Cold Expansion of Fastener Holes: Measurement, Eigenstrain, and Process Finite Element Modeling

Journal

Journal of Engineering Materials and Technology, 139(4)

ISSN

0094-4289

Authors

Ribeiro, Renan L
Hill, Michael R

Publication Date

2017-10-01

DOI

10.1115/1.4037021

Authors' version of paper to appear in: ASME Journal of Engineering Materials and Technology.
http://dx.doi.org/10.1115/1.4037021

Residual Stress from Cold Expansion of Fastener Holes: Measurement, Eigenstrain, and Process Finite Element Modeling

Renan L. Ribeiro
Michael R. Hill (mrhill@ucdavis.edu)

Department of Mechanical and Aerospace Engineering,
University of California, One Shields Avenue, Davis, CA 95616

Submitted to Journal of Engineering Materials and Technology January, 2017
Accepted April, 2017

ABSTRACT

Cold expansion (CX) is a material processing technique that has been widely used in the aircraft industry to enhance fatigue life of structural components containing holes. CX introduces compressive hoop residual stresses that slow crack growth near the hole edge. The objective of this paper is to predict residual stresses arising from cold expansion using two different finite element (FE) approaches, and compare the results to measurement data obtained by the contour method. The paper considers single-hole, double-hole, and triple-hole configurations with three different edge margins. The first FE approach considers process modeling, and includes elastic-plastic behavior, while the second approach is based on the eigenstrain method, and includes only elastic behavior. The results obtained from the FE models are in good agreement with one another, and with measurement data, especially close to the holes, and with respect to the effect of edge margin on the residual stress distributions. The distribution of the residual stress and equivalent plastic strain around the holes is also explored, and the results are discussed in detail. The eigenstrain method was found to be very useful, providing generally accurate predictions of residual stress.

Keywords: Cold expansion, residual stress, finite element analysis, eigenstrain

1. INTRODUCTION

The presence of holes in structural components is known to create local stress concentrations that become susceptible to fatigue failure. One of the methods to mitigate this effect is the cold expansion (CX) process, which introduces compressive residual hoop stress around the hole, and enhances fatigue life by slowing near-hole crack growth. The CX process involves pulling an oversized tapered mandrel through the hole, which induces plastic strain near the hole. Upon removal of the mandrel, the surrounding material undergoes elastic recovery,

producing a compressive residual stress field around the hole. In practice, the hole is reamed to the required size following CX. Figure 1 illustrates the split-sleeve CX process [1], which uses a split sleeve within the hole to ensure uniform radial expansion, and has been widely adopted in the aircraft and rotorcraft industries. A review of CX technology is presented in [2], and an useful overview of residual stress processes, including key research on CX, is given by McClung [3].

Many studies have been conducted to investigate the effect of CX-induced residual stress on fatigue and fracture. Cathey and Grandt [4] performed fatigue crack growth tests and fracture mechanics analysis in aluminum samples with CX holes, and found significant improvement in fatigue life compared to samples without CX. Petrak and Stewart [5] performed constant amplitude fatigue tests in aluminum samples and observed significant retardation of growth of preexisting cracks emanating from CX fastener holes. Rufin [6] presents test data showing that CX can result in fatigue life extension in a wide range of situations (e.g., noncircular holes, low edge margins, and components subjected to high operating temperatures). Chandawanich and Sharpe [7] performed an experimental study of fatigue crack initiation and growth from CX holes in samples made from 7075-T6 aluminum sheet and observed a significant decrease in crack growth rate in CX samples compared to samples without CX, but no effect on crack initiation. Ball and Lowry [8] performed fatigue crack growth experiments under constant and variable amplitude loading, and observed significant increases in fatigue life (total of initiation and growth) for samples with CX. These studies used 3% to 5% CX, where the percentage represents the amount by which the hole radius increases as the mandrel is pulled through the hole (at maximum expansion). Chakherlou and Vogwell [9] conducted an analytical and experimental study regarding CX holes. The experimental results showed a significant

improvement in fatigue life of CX samples compared to as-drilled samples (generally by a factor of 10 in the number of cycles to failure). Boni et al. [10] performed fatigue crack initiation and fatigue crack growth tests on 7075-T73 aluminum samples with CX, and found a remarkable increment in fatigue life due to the split sleeve cold expansion process, reaching 100 times more cycles to failure in the case of samples with double CX (i.e., CX applied twice, in opposite directions) as compared to samples not subjected to CX. Clearly, residual stresses arising from CX have a highly beneficial effect on fatigue behavior, particularly on the growth of fatigue cracks that initiate at the hole.

Given the significant effect of CX-induced residual stress on fatigue, it is important to accurately determine residual stresses from CX to provide input for fatigue crack growth analysis. Modeling tools that allow for accurate and rapid prediction of residual stress from CX are very desirable, but are not yet used in routine structural integrity assessments, even though the CX process has been applied widely for several decades.

The contour method has been successfully used to measure residual stress in cold-expanded holes [1,11]. This method includes three general steps: cutting the sample in half to relieve residual stress on a plane through the sample, measurement of the deformed shape of the cut-plane, and calculation of pre-cut residual stress using a three-dimensional elastic finite element (FE) analysis. More information about the contour method is given by Prime and DeWald [12]. The major benefit of contour for CX holes is that it provides a two dimensional map of hoop residual stress in the vicinity of the hole, which is directly useful when assessing the effect of residual stress on fatigue crack growth.

While residual stress measurement data are useful, it is also desirable to have modeling tools that predict residual stress for a broad range of geometry. One way to predict residual stress

from CX is to use the eigenstrain method. The term eigenstrain was initially suggested by Mura [13], and eigenstrain methods have been used by several authors to evaluate residual stress fields arising from material processing [14–16]. According to DeWald and Hill [14], eigenstrain can be considered an incompatible inelastic strain distribution that causes a given residual stress field, and does not satisfy geometric (strain) compatibility. An eigenstrain field can be determined from limited residual stress measurement data through an approach based on the superposition of the residual stress, as pursued in [14], or through an inverse method [17,18]. Once the correct eigenstrain distribution is determined, an elastic stress analysis reconstructs the residual stress field.

Another way to predict residual stress from CX is direct process modeling, which has appeared several times in the literature. For example, Ismonov et al. [1] used an elastic-plastic, three-dimensional finite element model to predict residual stress from split-sleeve CX in a thin rectangular aluminum sheet of 7075-T6 with a centrally located hole. The sleeve was modeled as purely elastic and the mandrel was assumed a rigid body. The authors evaluated the effects of friction and prescribed boundary conditions and compared the model results to contour method measurements. Kim et al. [19] used a simplified elastic-plastic finite element model to predict residual stresses resulting from CX of two adjacent holes, but did not provide comparison against measurement data. Boni et al. [10] described a three-dimensional FE analysis for CX and compared model results to measurements (from Sachs method). The prior work shows that process model outputs typically have limited agreement with measured residual stress fields, which calls for further research. It is important to recognize that process models of cold expansion are non-linear and time-consuming, with outputs specific to a given geometry. In

contrast, eigenstrain models are linear, and can be applied rapidly to complex geometry, but the linear formulation can limit applicability when considering a wide range of configuration.

A recent set of residual stress measurement data obtained with the contour method [20] provides an opportunity to explore eigenstrain and process modeling for CX holes. In a sustained campaign of experiments, measurements were performed on single-hole, double-hole, and triple-hole configurations. In all cases, the samples consisted of square plates with side length of 101.6 mm (4 inch), and thickness of 6.35 mm (0.25 inch). Our work focuses on results obtained for the samples that had 3% expansion applied to holes of diameter D = 12.7 mm (0.5 inch). One of the objectives of the work presented in [20] was to evaluate the effect of the edge margin, e/D, which is a ratio of the distance from the center of the hole to the edge of the plate, e, to hole diameter, as well as the effect of nearby holes on residual stress. For the single-hole configuration, the hole is located at the center of the sample, and as a result e/D = 4.0. The 2-hole configurations were symmetrical, with three different values of edge margins: e/D = 2.0, 1.5, and 1.2. The 3-hole configuration is equivalent to the 2-hole configuration with e/D = 1.2, but with the addition of a hole in the center of the plate. Figure 2 shows samples having e/D = 1.2, with the measurement plane shown as a dashed line. Figure 3a and Figure 3b show hoop residual stress obtained for all 2-hole configurations inward and outward from the holes, along with the results from the single hole configuration (e/D = 4.0). The residual stress is plotted on a path passing through the center of the holes, and taken at the mid-thickness of the plates. Figure 3a shows that the compressive stress at the hole edge is similar for all edge margins, but the size of the compressive region decreases as the edge margin decreases. Outward from the holes (Figure 3b), the magnitude of the compressive residual stress at the hole edge is also similar for all edge margins, but tensile residual stress away from the hole becomes larger as the edge margin

decreases. Consequently, the size of the compressive region decreases as the edge margin decreases. The measurement results obtained for the 3-hole configuration with e/D = 1.2 are shown in Figure 4, along with measured residual stress for the single-hole configuration. The size of the compressive zone is significantly decreased compared to the single-hole configuration, especially along the path from the outer holes inward. As for the 2-hole configurations, tensile residual stress exists near the edge of the plate, at levels significantly higher than for the single-hole at the plate center. While the literature has a number of publications describing process modeling of CX, there is a lack of published work addressing the effects of edge margin and including comprehensive validation against measurement data. There is also a lack of published work on eigenstrain models for CX holes.

The objective of this paper is to use FE models to predict residual stress arising at CX holes while comparing model results to measured residual stress data. The present models are simplified, assuming two-dimensional plane stress conditions. First, a process model (elastic-plastic) is used to determine residual stress in the single-hole, 2-hole, and 3-hole configurations described above. The elastic-plastic models include a flow curve derived through an iterative process involving the measured residual stress for the single-hole configuration. Second, an eigenstrain model is used. The required eigenstrain distribution is derived by an inverse technique using measured residual stress for the single-hole configuration. The eigenstrain field is then used to estimate residual stress for the 2-hole and 3-hole configurations. The results from both FE approaches are compared to one another and to the measurement data, and important aspects of the model results are discussed.

2. METHODS

2.1. Process modeling

The CX process model uses a plane stress elastic-plastic FE analysis with applied 3% radial expansion of the holes. The choice of 2D plane stress analysis was due to its simplicity, and was also an attempt to quantify the accuracy that can be obtained with simplified 2D models. This choice is further discussed in section 4.3. The elastic-plastic FE analysis was carried out using a commercial code [21]. A flow curve for 2024-T351 aluminum alloy describing the strain hardening for metal plasticity is provided by Bai and Wierzbicki [22], and is used here to provide an initial estimate of the residual stress field arising from cold expansion. The flow curve in [22] was determined using smooth round bar tensile tests and is of the form of a power-law function

$$\bar{\sigma} = 908(0.0058 + \bar{\epsilon}_p)^{0.1742} \text{ MPa} \quad (1)$$

where $\bar{\sigma}$ and $\bar{\epsilon}_p$ represent the flow stress and equivalent plastic strain, respectively. This flow curve is shown in Figure 5a, and was used in an initial FE analysis for determination of the residual stress from CX.

The geometry of the single-hole FE model is shown in Figure 6, along with a polar coordinate system with origin at the center of the hole. In addition, a rectangular coordinate system was used as indicated in the figure, with the same origin. Because of symmetry of geometry and loading, a quarter-model was used with two symmetry boundary conditions, as indicated Figure 6. The FE mesh had two-dimensional, eight-node biquadratic, plane stress quadrilateral elements, and was uniform around the hole and highly refined (elements adjacent to the hole had side length 0.016 *D*). The CX process was simulated by applying a radial displacement to nodes on the hole edge, with magnitude equal to 3% of the initial radius in a first

analysis step, and allowing for plastic deformation to occur. A second step in the analysis released the applied radial displacement, and followed relaxation to a traction-free condition of residual stress. Figure 5b shows the final hoop residual stress along the line y = 0 and compares it to the measured residual stress. The large differences between model and measurement in this plot are similar to those in other published CX simulations (e.g., [1] and [10]), all of which report using a flow curve derived from uniaxial tensile tests.

Given the significant differences between the process model results and the measurement, an iterative process was used to determine a flow curve that allows the FE process model to output a stress field that matches the measured residual stress. During this iterative process, points on the flow curve were manually adjusted. Adjustments were based on trends obtained in the resulting residual stress from systematic changes in areas of interest of the flow curve, and eventually provided process model results that match the measured residual stress. The adjusted flow curve (found by iteration) is then used to predict residual stress arising from cold expansion for the 2-hole and 3-hole configurations.

The 2-hole configurations analyzed in this study had edge margins (e/D) of 2.0, 1.5, and 1.2, since contour method data are available for these configurations. In order to evaluate the effect of sequential expansion of the holes, all 2-hole models had one symmetry boundary condition (along y = 0). The hole on the left side of the plate is called hole 1, while the hole on the right is called hole 2. In all 2-hole FE models, hole 1 was expanded first by applying a 3% expansion (radial displacement boundary condition), and releasing the applied displacements. Subsequently, hole 2 was expanded, and the radial displacement was released to provide the final residual stress. The FE models for different edge margins had the same boundary condition and geometry, differing only in the positions of the holes relative to the plate edges. The residual

hoop stress at hole 2 is plotted along the radial direction both inward (θ = 180°) and outward (θ = 0°) from the holes, and the results compared to values obtained by the contour method.

Similar to the 2-hole FE models, the 3-hole configuration with e/D = 1.2 was modeled as a half-model with one symmetry boundary condition and sequential expansion of the holes. In this case, the left hole is called hole 1, while the center and right holes are called hole 2 and hole 3, respectively. Hole 1 is expanded first, followed by hole 2 and then hole 3. The resulting residual stresses inward and outward from the right hole will be extracted along the line y = 0, and will be compared to the measurement values obtained by the contour method.

2.2. Eigenstrain modeling

The unknown eigenstrain distribution was derived from the measured hoop residual stress values using an inverse method. In this approach, the eigenstrain is assumed to be described by a series expansion of basis functions, and the basis function coefficients are determined by a least squares inversion that minimizes the disagreement between the model prediction of residual stress and the measurement data. DeWald and Hill [18] have successfully used the inverse eigenstrain method for multi-axial contour method, where the eigenstrain distribution was derived from measured average displacements. A similar approach was pursued by Kartal et al. [17] to derive an eigenstrain distribution and predict residual stresses in welded plates. Jun et al. [23] used an inverse eigenstrain analysis based on residual strain measurements to study non-uniformly shaped shot-peened stainless steel samples.

Here, only the hoop eigenstrain component was considered, since it was found to be capable of reproducing the residual stress field from CX. The inverse eigenstrain analysis considers a polar coordinate system with origin at the center of the hole. The eigenstrain characterizes the plastic strain resulting from the cold expansion process, and is taken to have

finite values close to the hole, and to be zero beyond a specific radial distance from the hole. The model assumes an axisymmetric, one-dimensional hoop eigenstrain $\varepsilon^*_{\theta\theta}(r)$ (only a function of the radial position, r) field that can be expressed as a power series

$$\varepsilon^*_{\theta\theta}(r) = \sum_{i=3}^{m} A_i[(r_{max} - r)/(r_{max} - R)]^i \tag{2}$$

where $\varepsilon^*_{\theta\theta}(r)$ is the unknown eigenstrain distribution, r is radial distance from the center of the hole, r_{max} is the radial zone of influence of cold expansion, $R = D/2$ is the hole radius, and A_i represent unknown coefficients to be determined. The power series expansion starts at $i = 3$ so that the eigenstrain is zero at r_{max}, and has zero first and second derivatives at r_{max}. In this study, r_{max} is taken to be $4R$. For $r \geq r_{max}$, the hoop eigenstrain component is taken to be zero.

With the series representation in Eq. (2), the determination of eigenstrain reduces to finding the $m - 2$ coefficients of the power series. These coefficients are found from the measured hoop residual stress, $\tilde{\sigma}_{\theta\theta}(r)$, by solving an inverse problem. Since the eigenstrain model is elastic, superposition allows the hoop residual stress to be expressed as a linear combination of the unknown basis coefficients

$$\sigma_{\theta\theta}(r_k) = \sum_{l=1}^{m-2} A_l C_{kl} \tag{3}$$

where C_{kl} is the hoop residual stress at $r = r_k$ for an eigenstrain distribution given by $[(r_{max} - r)/(r_{max} - R)]^{l+2}$. C_{kl} is called a compliance matrix, and is constructed using linear elastic finite element models. Each basis function from Eq. (2) is applied to a single-hole model

as an eigenstrain distribution using thermal strains. The FE models were quarter-models, with two symmetry boundary conditions identical to those used for the elastic-plastic model. The analysis was performed by defining a distribution of anisotropic thermal expansion coefficients equal to the desired eigenstrain distribution, and imposing a unit temperature increase in the whole model, as described earlier by DeWald and Hill [18]. An equilibrium step is taken and the resulting hoop residual stress from each eigenstrain basis function is extracted along the line θ = 0°. The compliance matrix C_{kl} has k rows (number of stress evaluation points) and $m - 2$ columns (number of basis functions). Here, residual stress measurement data are available at $k = 90$ points along the line $y = 0$, from $x/R = 1$ to 8. Eq. (3) can be re-written in matrix-vector form as

$$\{\sigma\} = [C]\{A\} \tag{4}$$

where $\{\sigma\}$ is a column vector of hoop residual stress, $[C]$ is the compliance matrix and $\{A\}$ is a column vector of the unknown coefficients. Typically, the number of measurement points is larger than the number of assumed polynomial terms $m - 2$, so that $\{A\}$ can be determined from a vector of measured residual stress $\{\tilde{\sigma}\}$ using the pseudo-inverse

$$\{A\} = ([C]^T[C])^{-1}[C]^T\{\tilde{\sigma}\}. \tag{5}$$

Having the coefficients $\{A\}$, the eigenstrain distribution is fully defined from Eq. (2). Application of the eigenstrain model consists of introducing the known eigenstrain field in an elastic model of the 2-hole or 3-hole configurations, and computing the equilibrium state of residual stress.

3. RESULTS

Figure 7a shows the initial flow curve used in the FE process model, an example flow curve iteration, and the final adjusted flow curve obtained from iteration, while Figure 7b shows the resulting hoop residual stress ($\sigma_{\theta\theta}$). The log scale on x/R in Figure 7b was used to facilitate visualization of the stress from different flow curves close the edge of the hole. Several iterations were required to obtain the final adjusted flow curve, with only a single iteration shown for illustration. It is interesting to note that the final adjusted flow curve is significantly different from the one derived from uniaxial test data. This will be discussed later. Figure 7b shows clearly that the final adjusted flow curve provides residual stresses that agree with the contour measurement.

The eigenstrain found from the inverse analysis is shown in Figure 8a. The eigenstrain field assumes four terms in the series (i.e., $m = 6$), with coefficients A_i of 1728, 8952, -40970, and 40610 με for $i = 3$, 4, 5, and 6, respectively. Applying the eigenstrain distribution from Figure 8a using anisotropic thermal strain in a single-hole FE model (geometry and boundary conditions of Figure 6) provides the hoop residual stress in Figure 8b (along $\theta = 0°$). It is clear that the eigenstrain determined with the inverse method reconstructs the measured residual stress. (An alternate approach to determine eigenstrain is suggested in [14], where the measured residual stress is considered a superposition of stress arising from the CX process and stress arising to satisfy equilibrium; additional work showed that this could also be applied here with results equivalent to those in Figure 8a.)

The hoop residual stresses ($\sigma_{\theta\theta}$) obtained from 2-hole FE models (elastic-plastic and eigenstrain) for e/D = 2.0 are shown in Figure 9a and Figure 9b, along with the measured residual stress. In the 2-hole elastic-plastic models, hole 1 corresponds to the left hole (first one to be expanded), and hole 2 corresponds to the right hole. The residual stresses are presented

along the paths going inward and outward from the holes, starting at the hole edge (x/R = 1). Inward from the holes (Figure 9a), very good agreement is observed between both FE models and the measurement data (within 27 MPa for the eigenstrain model, and 63 MPa for the elastic-plastic model). At the hole edge ($x/R = 1$), CX causes a maximum compressive residual stress. As distance from the hole increases, the compressive residual stress decreases, and the zero crossing point is near $x/R = 1.7$. Tensile residual stress arises far from the hole, as required for mechanical equilibrium. Figure 9b shows the residual stress outward from the holes, where there is agreement between the FE models and the measurement (within 38 MPa for the eigenstrain model, and 46 MPa for the elastic-plastic model), especially for $x/R \leq 2.3$. Further from the hole, the measurement results predict a shallow monotonic increase in the hoop residual stress, which is not captured by either of the FE models. The two FE models predict approximately the same behavior, and agree with one another along the whole path.

Figure 9c and Figure 9d show the hoop residual stress obtained from the 2-hole FE models and contour method for e/D = 1.5. Inward from the holes (Figure 9c), the results from the eigenstrain model have very good agreement compared to the measurement data (within 18 MPa). The elastic-plastic model provides results that have reasonable agreement with the measurement values (within 95 MPa), but exhibit visible differences. Outward from the holes (Figure 9d), the FE models predict residual stresses that agree well with the measurement up to x/R = 2 (especially the eigenstrain model), but deviate further from the holes (within 100 MPa for the eigenstrain model, and 89 MPa for the elastic-plastic model). Similar to results for e/D = 2.0, both FE models for e/D = 1.5 predict approximately the same behavior, and have general agreement along the full extent of the path up to the edge of the plate.

Results obtained for the 2-hole FE models with e/D = 1.2 are shown with contour method data in Figure 9e and Figure 9f. In this case, the holes are very close to the edge of the plate. Inward from the holes (Figure 9e), reasonable agreement is observed between the FE models and measurement data (within 68 MPa for the eigenstrain model, and 85 MPa for the elastic-plastic model), but there are some notable differences. The eigenstrain model generally has higher magnitude stress than the elastic-plastic model, and the measurement data falls closer to the elastic-plastic model at the hole edge but closer to the eigenstrain model near the tensile peak stress (x/R ~ 2). Outward from the holes (Figure 9f), the eigenstrain FE model predicts values of residual stress that agree very well with the measurement (within 25 MPa). The results from the elastic-plastic model exhibit the same trend, but the agreement with the measurement values is visibly less pronounced (within 114 MPa). These results are discussed further below.

The results obtained from the FE models for the 3-hole configuration with e/D = 1.2 are presented along paths from the center hole towards the outer holes, as well as inward and outward from the outer holes. Figure 10a shows the results obtained from the FE models along the path starting at the edge of the center hole, together with the measured data. Good general agreement is observed between the FE models and the measurement up to x/R ~ 1.9. Further from the center hole, the results from the FE models deviate from the measurements (within 64 MPa for the eigenstrain model, and 93 MPa for the elastic-plastic model), but agree well with each other. Again, the results from the two FE models exhibit the same behavior along the path, as for the 2-hole models. The measured tensile stress away from the hole is higher than for the FE models, as also occurred for the 2-hole configurations (e.g., in Figure 9b). The results obtained inward from the outer holes are presented in Figure 10b. In this case, there are some significant differences between the models and measurement data, especially further from the

holes (within 102 MPa for the eigenstrain model, and 175 MPa for the elastic-plastic model). The results from the FE models differ from one another near the hole, where the measured stress falls between the two models. Figure 10c presents the results on the path outward from the outer holes, where better agreement is observed between the measurement data and the FE models, especially the eigenstrain model (within 32 MPa for the eigenstrain model, and 120 MPa for the elastic-plastic model). This behavior was also observed for the 2-hole configuration with e/D = 1.2 (Figure 9f), and is further discussed below.

4. DISCUSSION

The results above demonstrate that finite element models are capable of producing residual stress estimates that correlate closely with measurement data in samples with CX holes. The good agreement depended on calibrating the models using experimentally measured residual stress in a plate having a single CX hole. In samples with the same CX process, but different configurations, in terms of numbers of holes, hole spacing, and edge margin, there was good agreement between results from the non-linear (elastic-plastic) physical process model, the linear eigenstrain model, and measured residual stress.

4.1. Effect of edge margin on plastic deformation

For small edge margin, the agreement between the non-linear and linear models is somewhat surprising. Proximity of the hole to the free edge might be expected to influence CX-imposed plasticity, which violates a key assumption of the eigenstrain model (i.e., that process-imposed strains are geometry independent). To more fully assess the situation, we document plastic deformation near the holes as a function of edge margin. Plastic deformation is quantified by equivalent plastic strain (PEEQ), extracted from the elastic-plastic process models along the paths used for evaluating residual stress. The equivalent plastic strain is calculated as

$$PEEQ = \int_0^t \sqrt{\frac{2}{3}\dot{\varepsilon}_{ij}^{pl}\dot{\varepsilon}_{ij}^{pl}}\, dt \tag{6}$$

where $\dot{\varepsilon}^{pl}$ is the time rate of the plastic strain tensor, and t reflects the (artificial) time scale used in the non-linear analysis. Results are shown in Figure 11a and Figure 11b, inward and outward from the holes for all edge margins, respectively, and also including the result for the single-hole model for comparison. There is noticeable change in PEEQ as a function of edge margin compared to the single-hole configuration. Inward from the holes, PEEQ decreases monotonically with position, and becomes zero around $x/R = 4$. This was not surprising, since CX induces plastic strains localized near the hole. PEEQ at the edge of the hole decreases as the edge margin decreases, and reaches a minimum value for e/D = 1.2. The behavior is very different along the path outward from the hole, as shown in Figure 11b. PEEQ at the edge of the hole decreases as the edge margin decreases, but PEEQ at the edge of the plate has the opposite trend, presumably due to the hole proximity to the plate edge. Edge margin e/D = 1.2 has the most significant differences in PEEQ compared to the single-hole configuration.

The changes in equivalent plastic strain as a function of the edge margin compared to the single-hole configuration give some insight about the differences observed between results from the two FE models. The eigenstrain model uses an eigenstrain distribution assumed independent of geometry, and derived from residual stress in the single-hole configuration. It should be expected that the eigenstrain model would be subject to error when plastic strain differs significantly from plastic strain for the single-hole. As the edge margin decreases, the elastic-plastic FE model shows that plastic strain around the hole is influenced by the edge margin.

Considering the residual hoop stresses inward from the holes in the 2-hole models (Figure 9a, Figure 9c, and Figure 9e), it is evident that as e/D decreases, the agreement between the eigenstrain and process models decreases. However, the differences in residual stress are rather small when compared to the differences in PEEQ with decreasing e/D, as seen in Figure 11a. Along the path outward from the holes, as e/D decreases (Figure 11b), PEEQ significantly deviates from that for the single-hole configuration, but the residual stress for the eigenstrain and process models are still in fairly close correspondence (Figure 9b, d, and f). The same observation applies for the results from the 3-hole configuration, where the eigenstrain and process models predict values of residual hoop stress in reasonable agreement (Figure 10c), even though the plastic strains are significantly different from the single-hole configuration. These observations suggest that the mechanics of the problem are somewhat complex.

4.2. Symmetry of stress fields

Another aspect of the results that is worth exploring is the symmetries of the hoop residual stress and PEEQ as a function of edge margin. For both single-hole FE models, hoop residual stress was found to be identical on $\theta = 0°$, 45°, and 90°, and so these results were judged as axisymmetric. The axisymmetry is consistent with the hole being sufficiently far from the boundaries of the plate and there being no features that affect the axial symmetry. PEEQ for the single-hole elastic-plastic model was also found to be axisymmetric. Figure 12a and Figure 12b show the hoop residual stress from the FE models with e/D = 2.0 along lines with varying angle from 0° to 180°, with in set contour plots to show the hoop residual stress fields (with scale from -600 to 200 MPa). The hoop residual stress is nearly axisymmetric around the hole for e/D = 2.0, but not when the edge margin decreases to e/D = 1.5, as seen in Figure 12c and Figure 12d, especially far from the hole. The hoop residual stress is nearly axisymmetric near the hole for

e/D = 1.5, up to x/R ~ 1.8 for both FE models, but differences occur further away from the hole. For e/D = 1.2, a lack of axisymmetry appears closer the hole, around x/R ~ 1.5 (Figure 12e and Figure 12f). The edge of the plate influences the residual stress distribution around the hole, and causes a lack of symmetry. The same behavior was noted for PEEQ in the elastic-plastic FE models. Figure 13a shows the results for e/D = 2.0, where the equivalent plastic strain is approximately axisymmetric. Again, a contour plot is included for illustration of the spatial variation of PEEQ (also included in the next figures). As e/D decreases, the lack of symmetry becomes more pronounced, as seen for e/D = 1.5 in Figure 13b, and especially for e/D = 1.2 (Figure 13c). For the 3-hole configuration, the hoop residual stress around the outer hole is shown in Figure 14a for the eigenstrain model, and in Figure 14b for the elastic-plastic model. There are significant differences between the residual stresses along different paths beyond x/R = 1.5. Around the center hole (Figure 14c and Figure 14d), the hoop residual stress is approximately axisymmetric. PEEQ was extracted from the 3-hole elastic-plastic model along the same paths, and exhibits similar behavior as for the stress. The values around the center hole are axisymmetric, as shown in Figure 15a, and are equivalent to the ones obtained from the single-hole model (except at the hole edge). This suggests that the outer holes are far enough from the center hole as to not cause lack of axial symmetry. Around the outer hole (Figure 15b), there is a lack of axial symmetry.

4.3. Flow curve obtained by iteration

The flow curve obtained by the iteration process described in the Methods section is worth further discussing. It is important to recognize that the triaxial stress state to which a sample is subjected, and not only the second stress invariant J_2, influences the resulting plastic flow, as illustrated by Gutscher et al. [24] when using the bulge test, and by Merklein et al. [25]

when using both bulge and compression tests. In order to understand the stress state at the vicinity of the hole during the cold expansion process, the stresses from the elastic-plastic model for the single-hole were evaluated as a function of the radial expansion. It is important to note that the initial flow curve (Figure 5a) was derived using a power function to fit data from uniaxial tensile tests of 2024-T351 samples [22]. To assess the stress state during cold expansion, the von Mises effective stress, q, and the hydrostatic pressure, p, were extracted at several positions on θ = 0 (including the edge of the hole, x/R = 1) as a function of hole expansion. The stress triaxiality, η, was calculated as $\eta = -p/q$. Figure 16 shows the stress triaxiality obtained for selected positions (x/R) during the expansion step. The stress triaxiality near the edge of the hole is very different than that in the uniaxial tension case, for which $\eta = 0.33$. Initially, the values are close to zero, which results from radial compressive stress (pressure) being equal to tensile hoop stress. As loading advances, the stress triaxiality becomes more negative, as a result of radial compression (negative) exceeding tensile hoop stress (positive). It is also interesting to observe that as the distance from the edge of the hole increases, the stress triaxiality values approach the uniaxial case, exactly reproducing it at the right-lower corner of the sample (x/R = 8).

The large difference in stress triaxiality at the hole edge compared to that in a uniaxial stress state (Figure 16) illustrates how different the loading caused by CX is from a uniaxial case. Bai and Wierzbicki [22] proposed a plasticity model that accounts for the effect of hydrostatic pressure on yield. The model is given by

$$\sigma_{yld} = \bar{\sigma}\left(\bar{\varepsilon_p}\right)[1 - c_\eta(\eta - \eta_0)] \tag{7}$$

where $\bar{\sigma}(\bar{\varepsilon_p})$ is the material flow curve from a reference test, η_0 is the stress triaxiality in the reference test (i.e., 1/3 for smooth round bar tensile test), and c_η is a material constant that needs to be calibrated for the specific material to provide the effect of hydrostatic pressure on flow stress. For 2024-T351, Bai and Wierzbicki reported c_η = 0.09 and an illustration of the use of this model for the indentation process was given by Prime [26]. To illustrate this effect on the initial flow curve used here, flow curves adjusted by the range of triaxiality at x/R = 1 shown in Figure 16 were determined using Eq. (7) and are shown in Figure 17, along with the adjusted flow curve that resulted from iteration. It is clear that including the effect of hydrostatic pressure present during CX elevates the flow curve (because of negative triaxiality), which brings the initial curve toward the final adjusted flow obtained from iteration. However, the adjusted flow curve has low strength at small plastic strain (< 0.005) that is not explained by the model, and so requires more investigation. Of course, the adjusted flow curve was made to match the measured residual stress for the single hole configuration. Uncertainty and experimental error in the measurement could therefore contribute to errors and uncertainties in the adjusted flow curve. It is also important to remember the assumption of 2D plane stress analysis used in all process models. This assumption leads to a flow curve that is only appropriate for the context of plane stress analysis. However, we confirmed that re-analysis of the single-hole configuration using plane strain produces only a minor change in residual stress. Three-dimensional analyses might require a different flow curve to match the measured residual stress in the single-hole configuration, and are recommended for future work.

4.4. Non-uniqueness of the adjusted flow curve

Another interesting point is the fact that different flow curves can provide the same residual stress distribution, so that the iteration-based adjusted flow curve is non-unique. For

illustration, a second flow curve was found having roughly twice the strength of the adjusted flow curve reported above. This flow curve is shown in Figure 18a and, when used in the single-hole process model, provides nearly the same hoop residual stress shown previously, as shown in Figure 18b. This may be surprising, and is due to the expansion problem being driven by deformation, and not load. To further illustrate this result, Figure 19 shows the evolution of the hoop stress during the CX simulation at selected radial locations obtained with each flow curve. In the x-axis, maximum expansion (end of step 1 in the analysis), and unloaded configuration (end of step 2 in the analysis) are indicated. At x/R = 1 (Figure 19a), we observe that the hoop stress peaks at different levels during the loading step depending on the flow curve used. However, after unloading is complete, the hoop residual stress ends up at approximately the same level. Similar behavior is observed at x/R = 1.5 (Figure 19b), and x/R = 6 (Figure 19c), indicating different hoop stress evolution during the loading step, but approximately same hoop residual stress left at the end of the unloading step. Other radial locations were analyzed and exhibited the same behavior, supporting the results shown in Figure 18b.

4.5. Significance of eigenstrain modeling

The eigenstrain FE models are elastic, and provide very similar results to the elastic-plastic models in all configurations considered in this paper. For all 2-hole configurations, at the edge of the hole (on the inward side), the eingenstrain models predict residual stress within 58 MPa of the measured stress, compared to 95 MPa for the elastic-plastic models. On the outward side, these numbers are 25 and 114 MPa, respectively. For the 3-hole configuration, residual stress from the eigenstrain model at the edge of the holes are within 41 MPa of the measured stress, and within 190 MPa for the elastic-plastic model. This suggests that the eigenstrain approach is a useful model for residual stresses arising from CX, and provides a way to study the

residual stress field without nonlinear modeling. In addition, the eigenstrain approach is valuable because it can be applied to a broad range of geometry rapidly, with the simplicity typical of elastic analysis.

5. CONCLUSION

This work describes the estimation of residual stress arising from CX in single-hole, double-hole, and triple-hole configurations using two different models, and compares the model results to residual stress measured with the contour method. Particular attention was devoted to the effects of neighboring holes and edge margin on the residual stress distributions. The first model was a process model, using an elastic-plastic flow curve adjusted to reconstruct measured residual stress for CX of a single-hole configuration. The second model was an eigenstrain model, using an inverse technique to determine a characteristic eigenstrain distribution from measured residual stress for a single-hole configuration. Computed residual stress from both approaches, for double and triple-hole configurations, had good agreement with measured residual stress data, especially near the edges of the holes. Further from the holes, the models were often anti-conservative, predicting tensile residual stresses lower than were measured. As the edge margin decreased, the FE models predict decreased size of the compressive region around the holes and higher magnitudes of tensile residual stress away from the holes, which is in agreement with the measurement data. With decreasing edge margin, the models also show distortions of the symmetries in hoop residual stress and equivalent plastic strain that are typical of holes with large edge margin. Both models were found to provide useful residual stress estimates. The model results give confidence in the effects of edge margin and neighboring holes on residual stress that were suggested in [20] based only on measurement data. Overall, this

work demonstrated the capabilities of both eigenstrain and process models in predicting residual stresses arising from CX for a variety of configurations.

REFERENCES

[1] Ismonov, S., Daniewicz, S. R., Newman J. C., J., Hill, M. R., and Urban, M. R., 2009, "Three Dimensional Finite Element Analysis of a Split-Sleeve Cold Expansion Process," J. Eng. Mater. Technol., **131**(3), p. 31007.

[2] Fu, Y., Ge, E., Su, H., Xu, J., and Li, R., 2015, "Cold expansion technology of connection holes in aircraft structures: A review and prospect," Chinese J. Aeronaut., **28**(4), pp. 961–973.

[3] McClung, R. C., 2007, "A literature survey on the stability and significance of residual stresses during fatigue," Fatigue Fract. Eng. Mater. Struct., **30**(3), pp. 173–205.

[4] Cathey, W. H., and Grandt A. F., J., 1980, "Fracture Mechanics Consideration of Residual Stresses Introduced by Coldworking Fastener Holes," J. Eng. Mater. Technol., **102**(1), pp. 85–91.

[5] Petrak, G. J., and Stewart, R. P., 1974, "Retardation of cracks emanating from fastener holes," Eng. Fract. Mech., **6**(2), pp. 275–282.

[6] Rufin, A. C., 1993, "Extending the fatigue life of aircraft engine components by hole cold expansion technology," J. Eng. gas turbines power, **115**(1), pp. 165–171.

[7] Chandawanich, N., and Sharpe, W. N., 1979, "An experimental study of fatigue crack initiation and growth from coldworked holes," Eng. Fract. Mech., **11**(4), pp. 609–620.

[8] Ball, D. L., and Lowry, D. R., 1998, "Experimental Investigation on the Effects of Cold Expansion of Fastener Holes," Fatigue Fract. Eng. Mater. Struct., **21**(1), pp. 17–34.

[9] Chakherlou, T. N., and Vogwell, J., 2003, "The effect of cold expansion on improving the fatigue life of fastener holes," Eng. Fail. Anal., **10**(1), pp. 13–24.

[10] Boni, L., Fanteria, D., Lanciotti, A., and Polese, C., 2013, "Experimental and analytical assessment of fatigue and crack propagation in cold worked open hole specimens," Fatigue Fract. Eng. Mater. Struct., **36**(9), pp. 930–941.

[11] Stuart, D. H., Hill, M. R., and Newman Jr, J. C., 2011, "Correlation of one-dimensional fatigue crack growth at cold-expanded holes using linear fracture mechanics and superposition," Eng. Fract. Mech., **78**(7), pp. 1389–1406.

[12] Prime, M. B., and DeWald, A. T., 2013, "The Contour Method," Practical Residual Stress Measurement Methods, John Wiley & Sons, Ltd, pp. 109–138.

[13] Mura, T., 1987, Micromechanics of defects in solids, Martinus Nijhoff, Dordrecht, Netherlands.

[14] DeWald, A. T., and Hill, M. R., 2009, "Eigenstrain-based model for prediction of laser peening residual stresses in arbitrary three-dimensional bodies Part 1: Model description," J. Strain Anal. Eng. Des., **44**(1), pp. 1–11.

[15] DeWald, A. T., and Hill, M. R., 2009, "Eigenstrain-based model for prediction of laser peening residual stresses in arbitrary three-dimensional bodies Part 2: Model verification," J. Strain Anal. Eng. Des., **44**(1), pp. 13–27.

[16] Correa, C., Gil-Santos, A., Porro, J. A., Díaz, M., and Ocaña, J. L., 2015, "Eigenstrain simulation of residual stresses induced by laser shock processing in a Ti6Al4V hip replacement," Mater. Des., **79**, pp. 106–114.

[17] Kartal, M. E., Kang, Y.-H., Korsunsky, A. M., Cocks, A. C. F., and Bouchard, J. P., 2016, "The influence of welding procedure and plate geometry on residual stresses in thick components," Int. J. Solids Struct., **80**, pp. 420–429.

[18] DeWald, A. T., and Hill, M. R., 2006, "Multi-Axial Contour Method for Mapping Residual Stresses in Continuously Processed Bodies," Exp. Mech., **46**(4), pp. 473–490.

[19] Kim, C., Kim, D.-J., Seok, C.-S., and Yang, W.-H., 2004, "Finite element analysis of the residual stress by cold expansion method under the influence of adjacent holes," J. Mater. Process. Technol., **153**–**154**, pp. 986–991.

[20] DeWald, A., Hill, M., VanDalen, J., Pilarczyk, R., Andrew, D., Thomsen, M., Carlson, S., and Marosok, D., 2013, "Residual Stresses from Cold Working of Aircraft Fastener Holes," The Aircraft Structural Integrity Program Conference, The Aircraft Structural Integrity Program Conference, Bonita Springs, FL.

[21] 2011, "ABAQUS/Standard, Version 6.11," Dassault Syst. Simulia Corp, p. Providence, RI, USA.

[22] Bai, Y., and Wierzbicki, T., 2008, "A new model of metal plasticity and fracture with pressure and Lode dependence," Int. J. Plast., **24**(6), pp. 1071–1096.

[23] Jun, T.-S., Venter, A. M., la Grange, C. P., Hofmann, F., Belnoue, J., van Heerden, P. R., Evans, A., and Korsunsky, A. M., 2009, "Eigenstrain analysis of non-uniformly shaped shot-peened samples," Procedia Eng., **1**(1), pp. 151–154.

[24] Gutscher, G., Wu, H.-C., Ngaile, G., and Altan, T., 2004, "Determination of flow stress for sheet metal forming using the viscous pressure bulge (VPB) test," J. Mater. Process. Technol., **146**(1), pp. 1–7.

[25] Merklein, M., and Gödel, V., 2009, "Characterization of the flow behavior of deep drawing steel grades in dependency of the stress state and its impact on fea," Int. J. Mater. Form., **2**(1), pp. 415–418.

[26] Prime, M. B., 2013, "Anisotropic and pressure-dependent plasticity modeling for residual stress prediction," Experimental and Applied Mechanics, Volume 4, Springer, pp. 415–427.

FIGURES

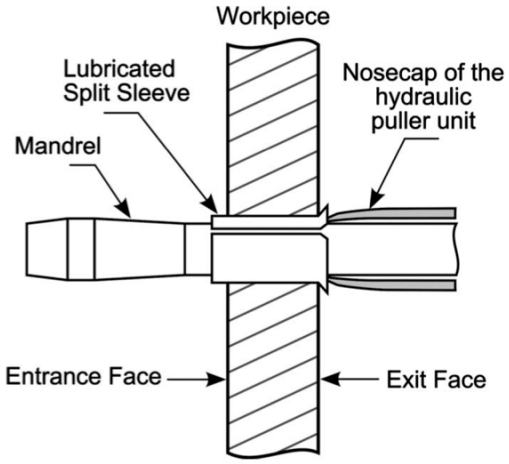

Figure 1 – Split-sleeve cold expansion process (from [1]*)*

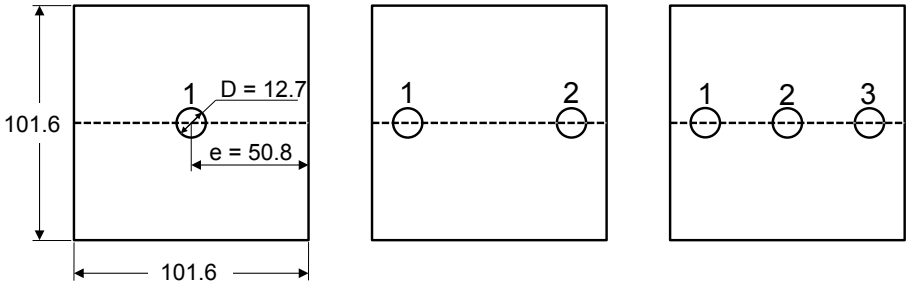

Figure 2 – Sample configurations and measurement plane used in [20] *(dimensions in mm; 2 and 3-hole configurations shown with e/D = 1.2)*

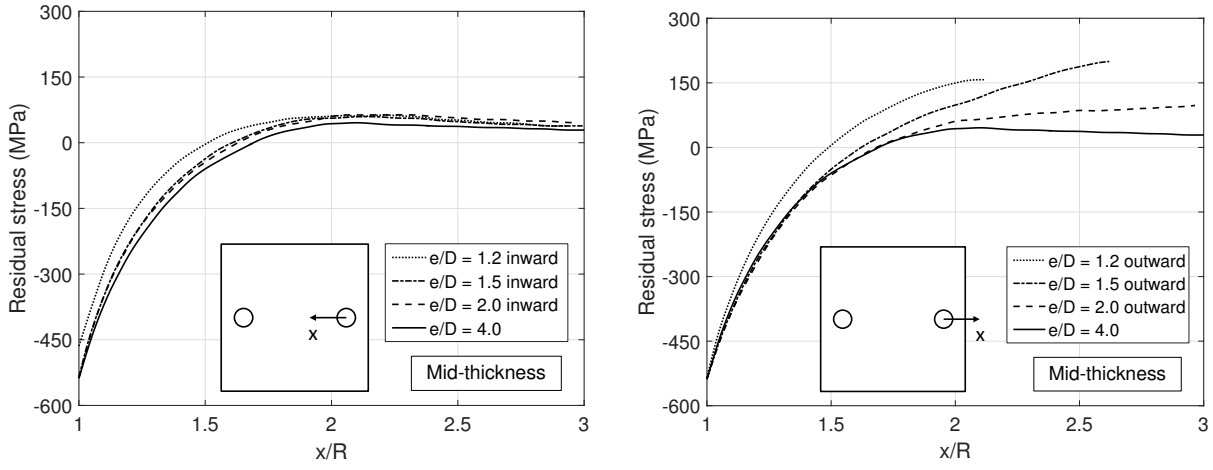

(a) (b)

Figure 3 – Hoop residual stress measured by the contour method in samples with two holes [20] *(a) inward from hole, (b) outward from hole*

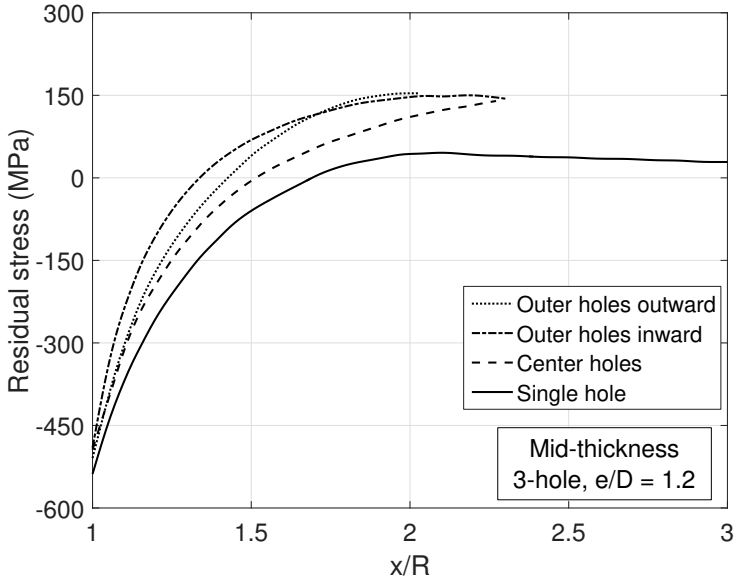

Figure 4 – Hoop residual stress measured by the contour method in 3-hole configuration [20]

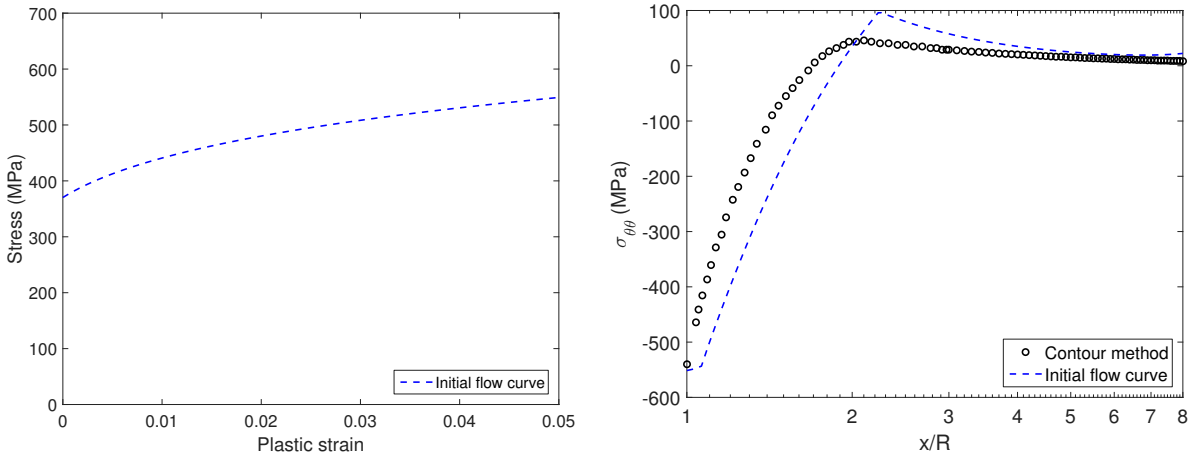

(a) (b)

Figure 5 – (a) Initial flow curve for 2024-T351, (b) resulting hoop residual stress ($\sigma_{\theta\theta}$)

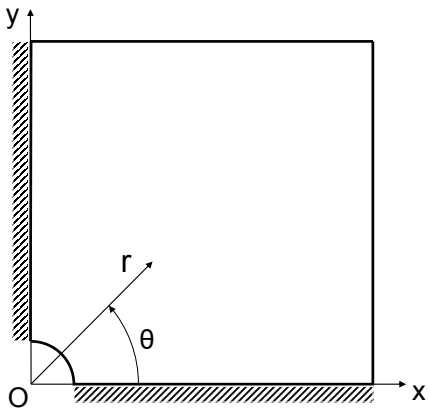

Figure 6 – Single-hole FE model and boundary conditions (hatches represent symmetry boundary conditions)

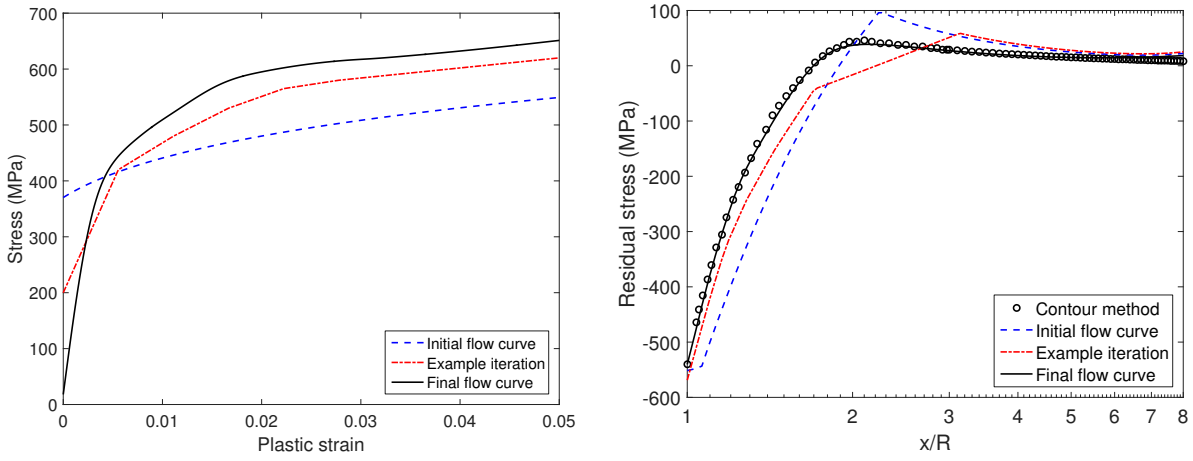

(a) (b)

Figure 7 – (a) Flow curves tested, (b) resulting hoop residual stress ($\sigma_{\theta\theta}$); note log scale on x/R

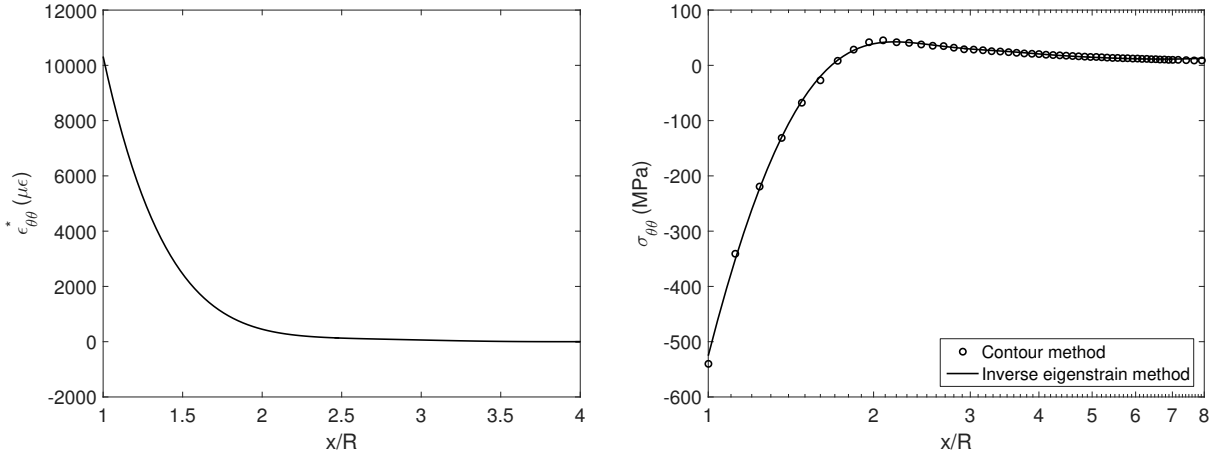

(a) (b)

Figure 8 – (a) Eigenstrain distribution obtained with inverse method, (b) resulting hoop residual stress ($\sigma_{\theta\theta}$)

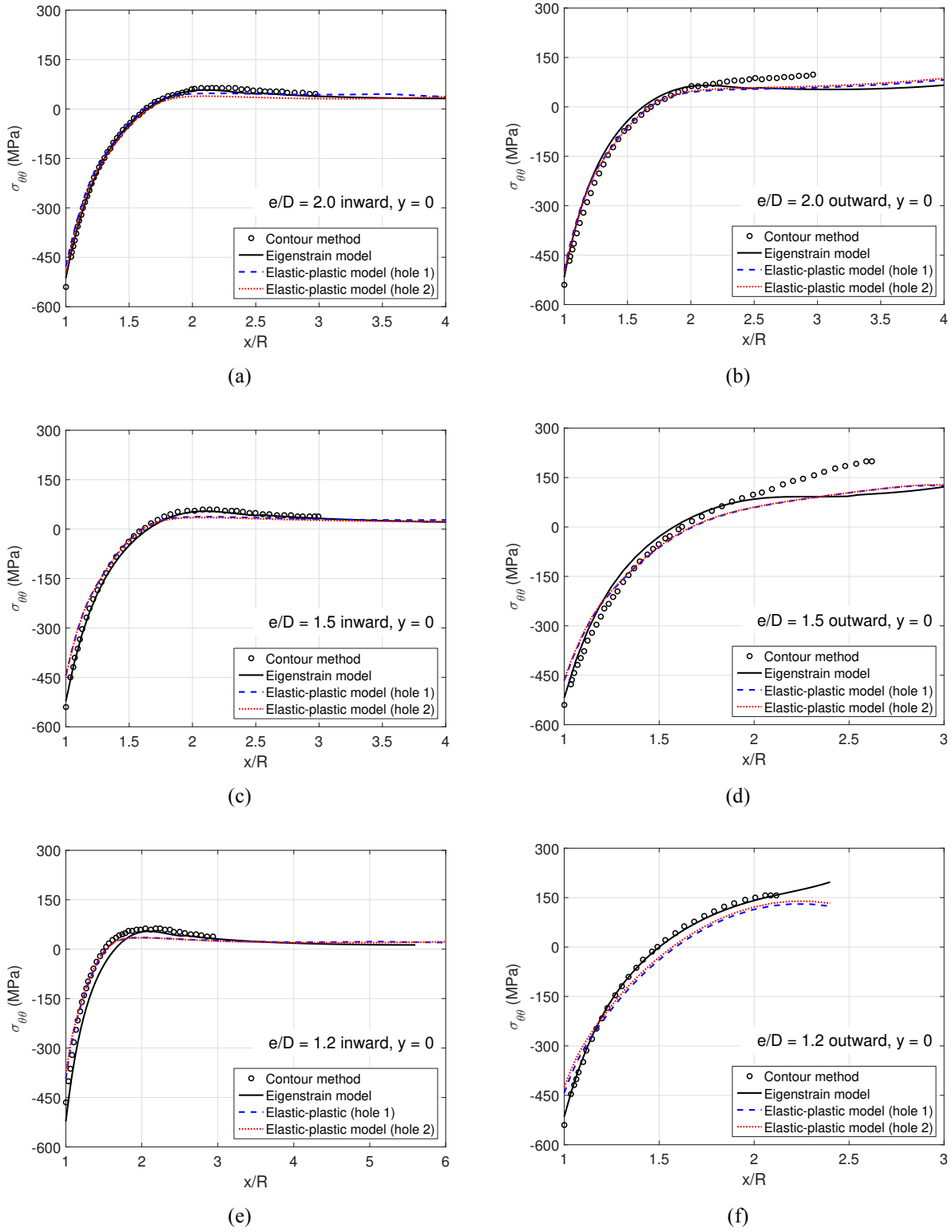

Figure 9 – Hoop residual stress for 2-hole samples (a) inward from holes (e/D = 2.0), (b) outward from holes (e/D = 2.0), (c) inward from holes (e/D = 1.5), (d) outward from holes (e/D = 1.5), (e) inward from holes (e/D = 1.2), (f) outward from holes (e/D = 1.2)

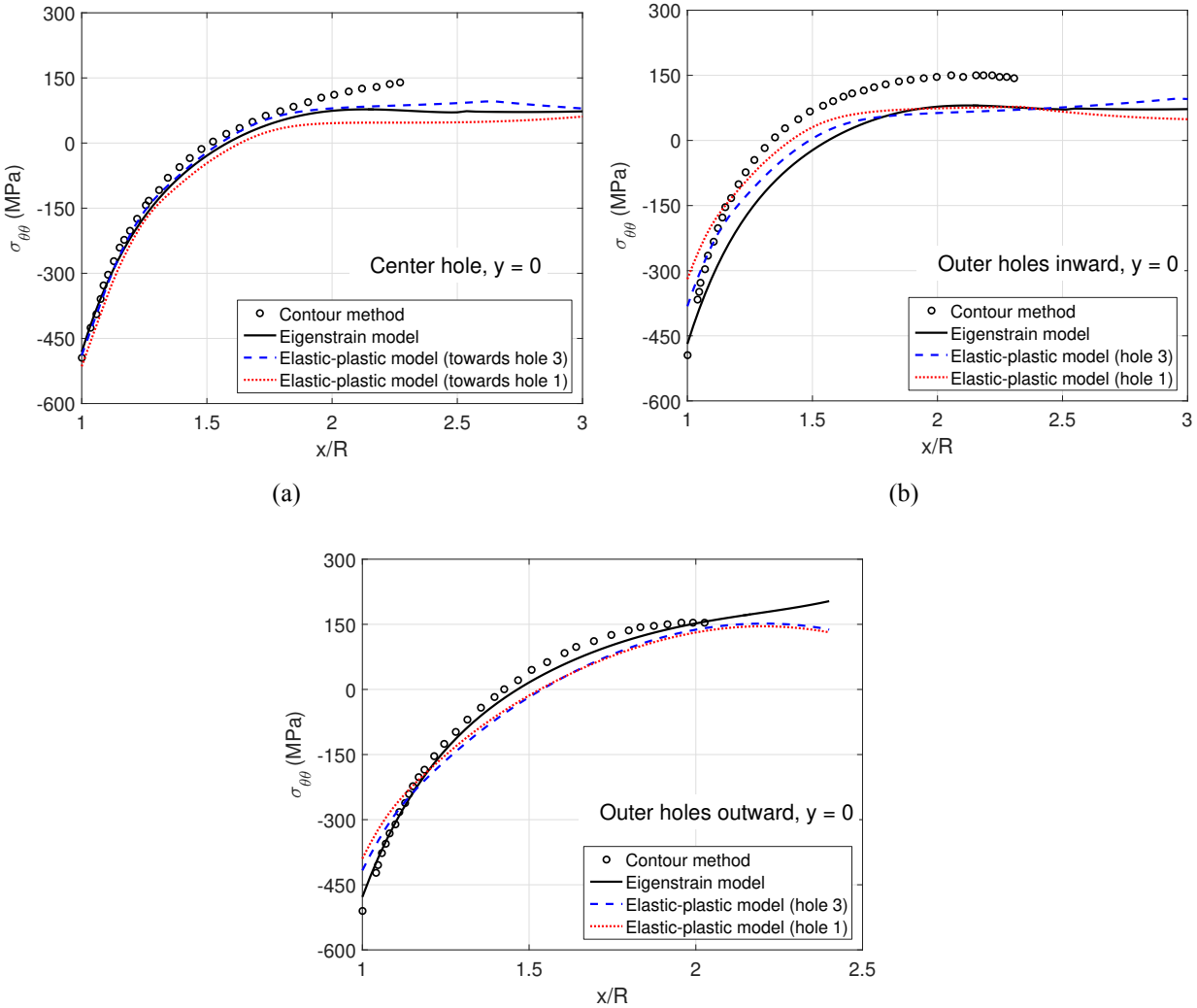

Figure 10 – Hoop residual stress from 3-hole configuration, e/D = 1.2 (a) center hole towards outer holes, (b) inward from outer holes, (c) outward from outer holes

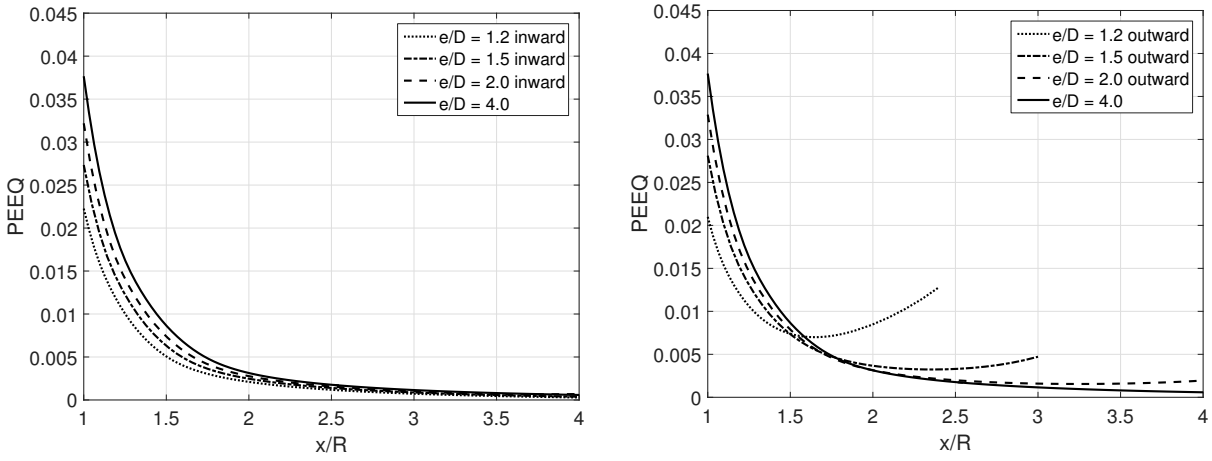

(a) (b)

Figure 11 – Equivalent plastic strain in 2-hole samples for all edge margins (a) inward from hole, (b) outward from hole

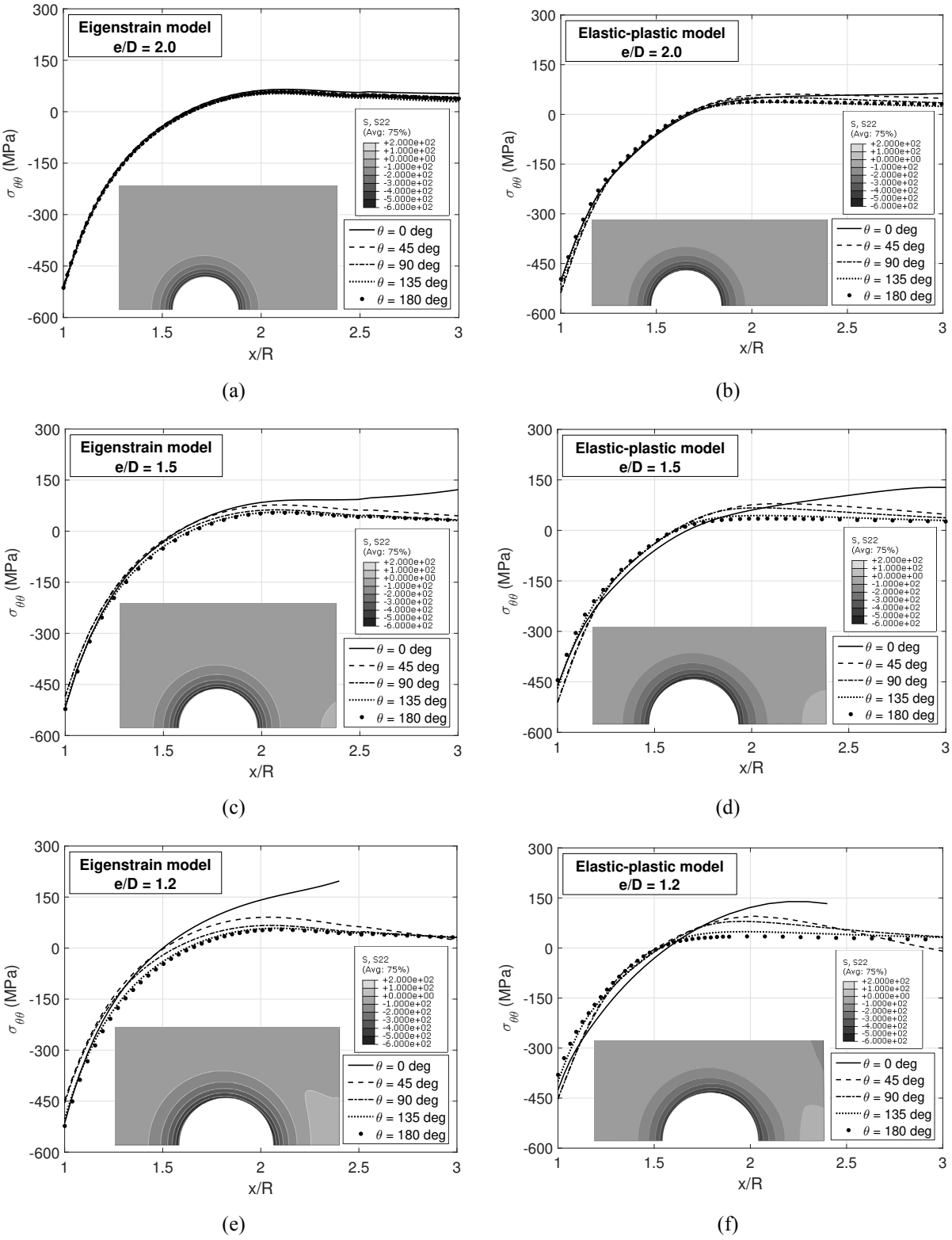

Figure 12 – Hoop residual stress from 2-hole configurations for varying angular position from (a) eingestrain FE model (e/D = 2.0), (b) elastic-plastic FE model (e/D = 2.0), (c) eingestrain FE model (e/D = 1.5), (d) elastic-plastic FE model (e/D = 1.5), (e) eingestrain FE model (e/D = 1.2), (f) elastic-plastic FE model (e/D = 1.2)

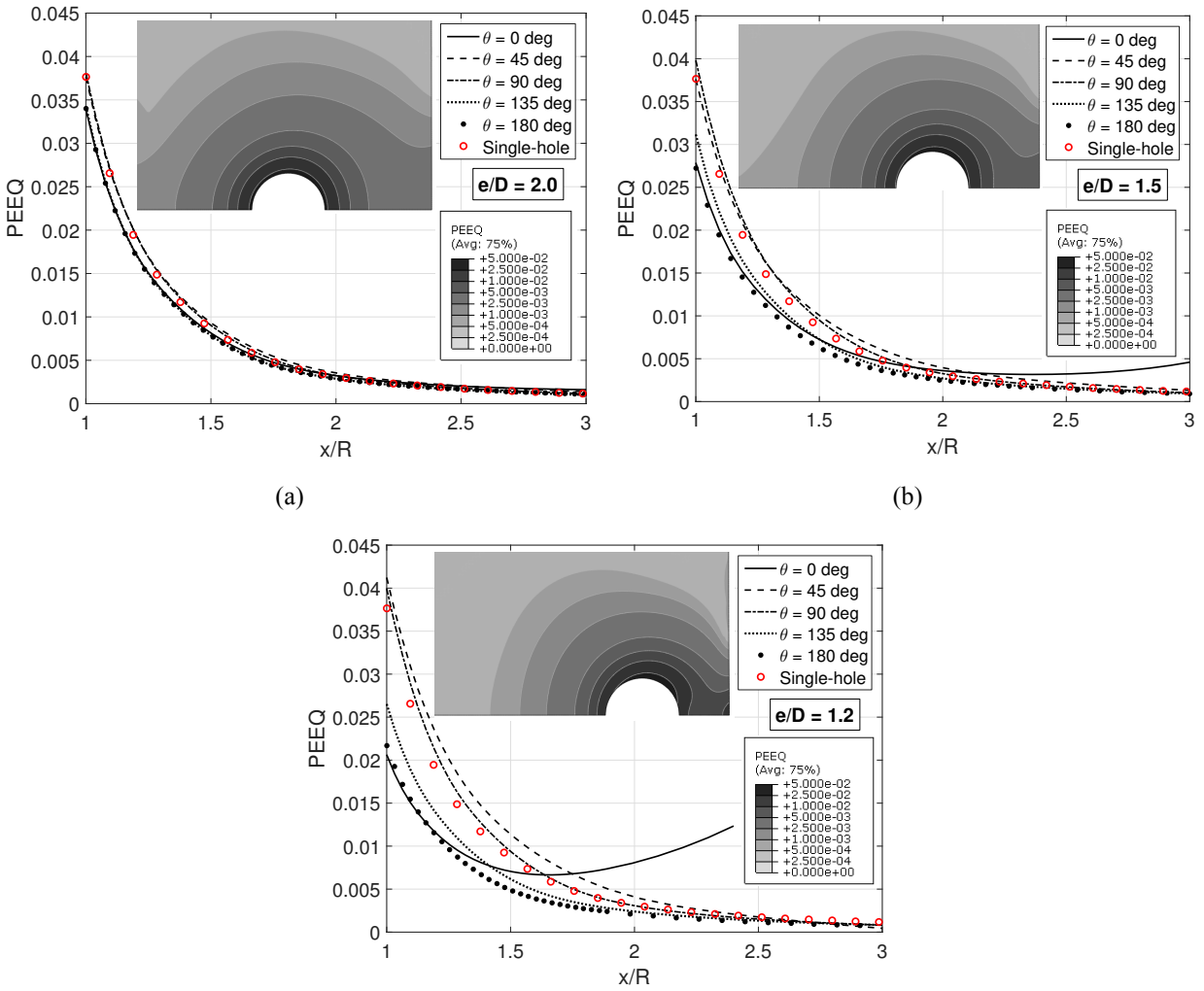

(a) (b)

(c)

Figure 13 – Equivalent plastic strain from 2-hole elastic-plastic FE model for varying angular positions (a) e/D = 2.0, (b) e/D = 1.5, (c) e/D = 1.2

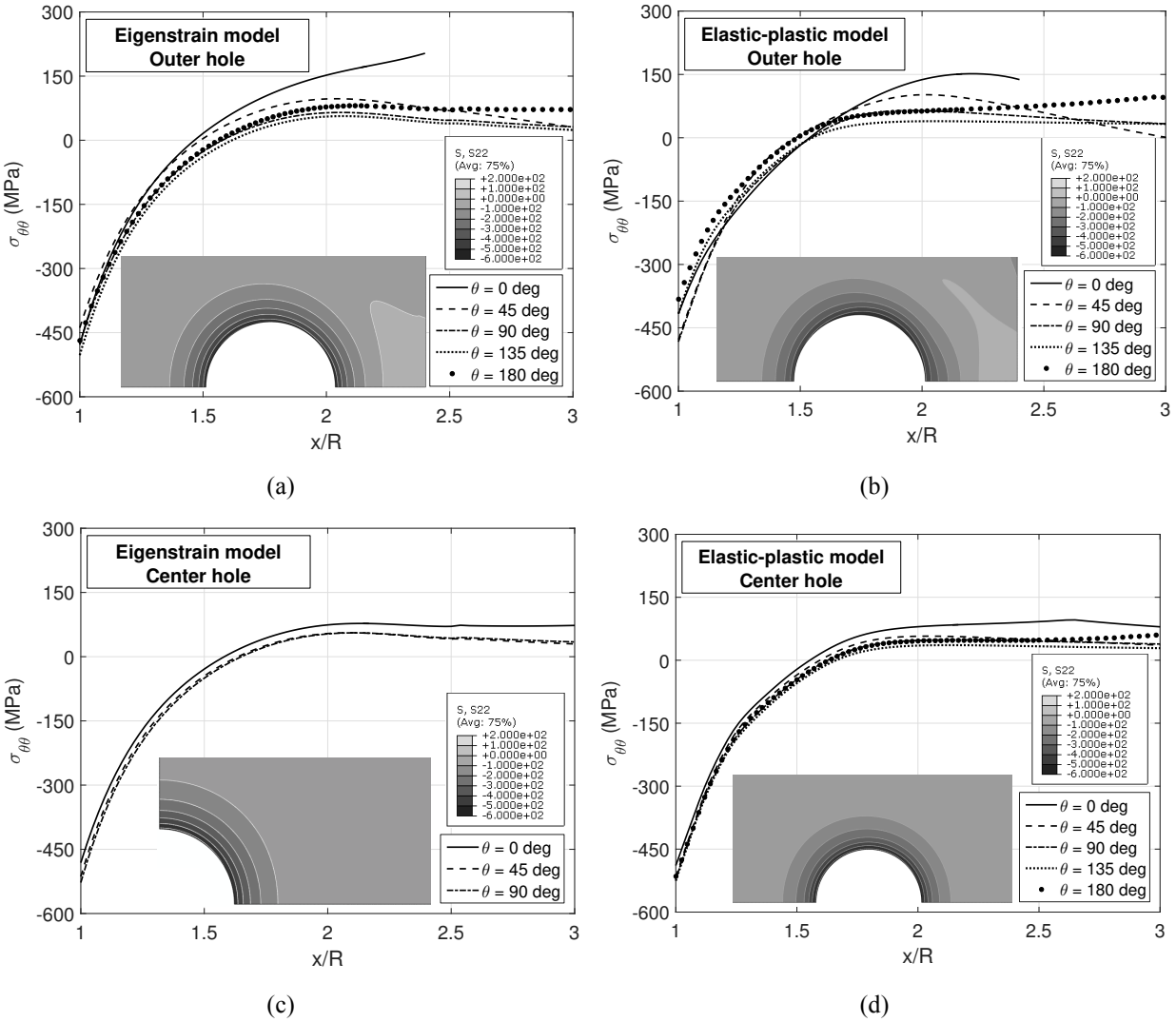

Figure 14 – Hoop residual stress from 3-hole configuration for varying angular position from (a) outer hole from eigenstrain FE model, (b) outer hole from elastic-plastic FE model, (c) center hole from eigenstrain FE model, (d) center hole from elastic-plastic FE model

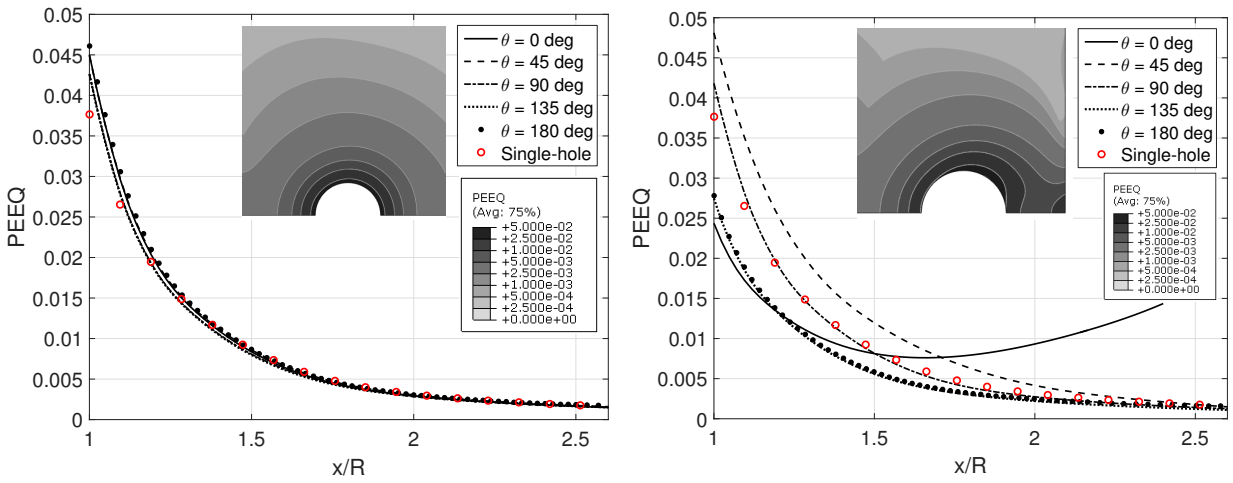

(a) (b)

Figure 15 – Equivalent plastic strain from 3-hole configuration for varying angular position from (a) center hole, (b) outer hole

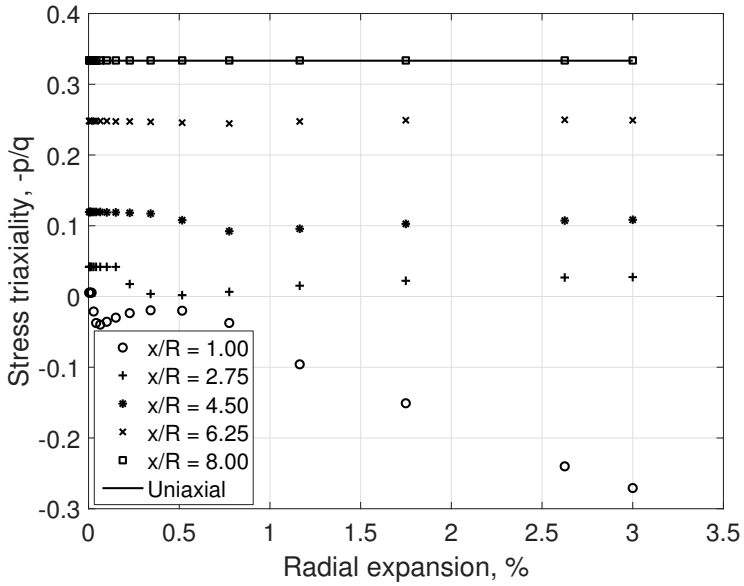

Figure 16 – Stress triaxiality versus hole expansion at different locations from single-hole elastic-plastic model with final flow curve

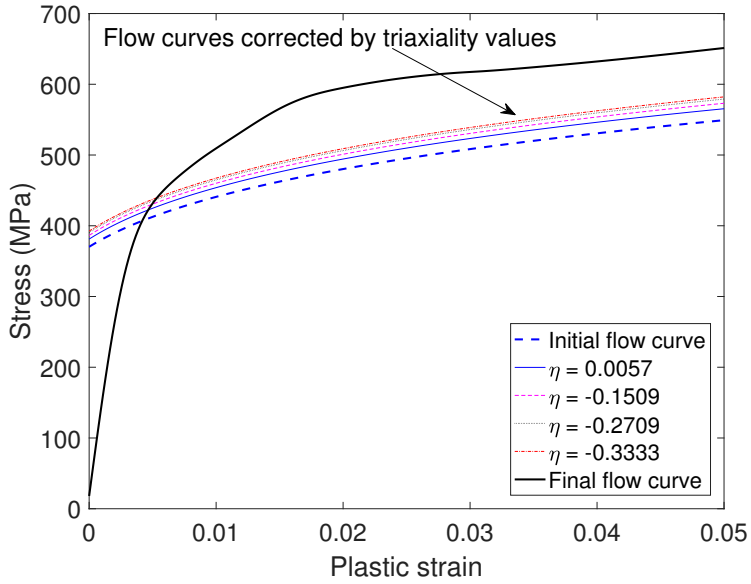

Figure 17 – Flow curves corrected by triaxiality values

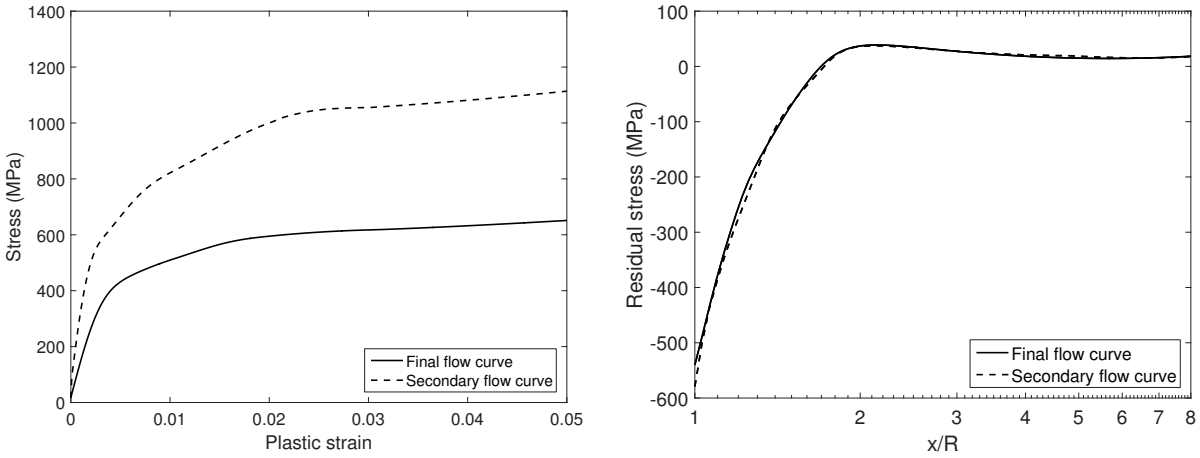

(a) (b)

Figure 18 – (a) Final and secondary flow curves, (b) resulting hoop residual stress

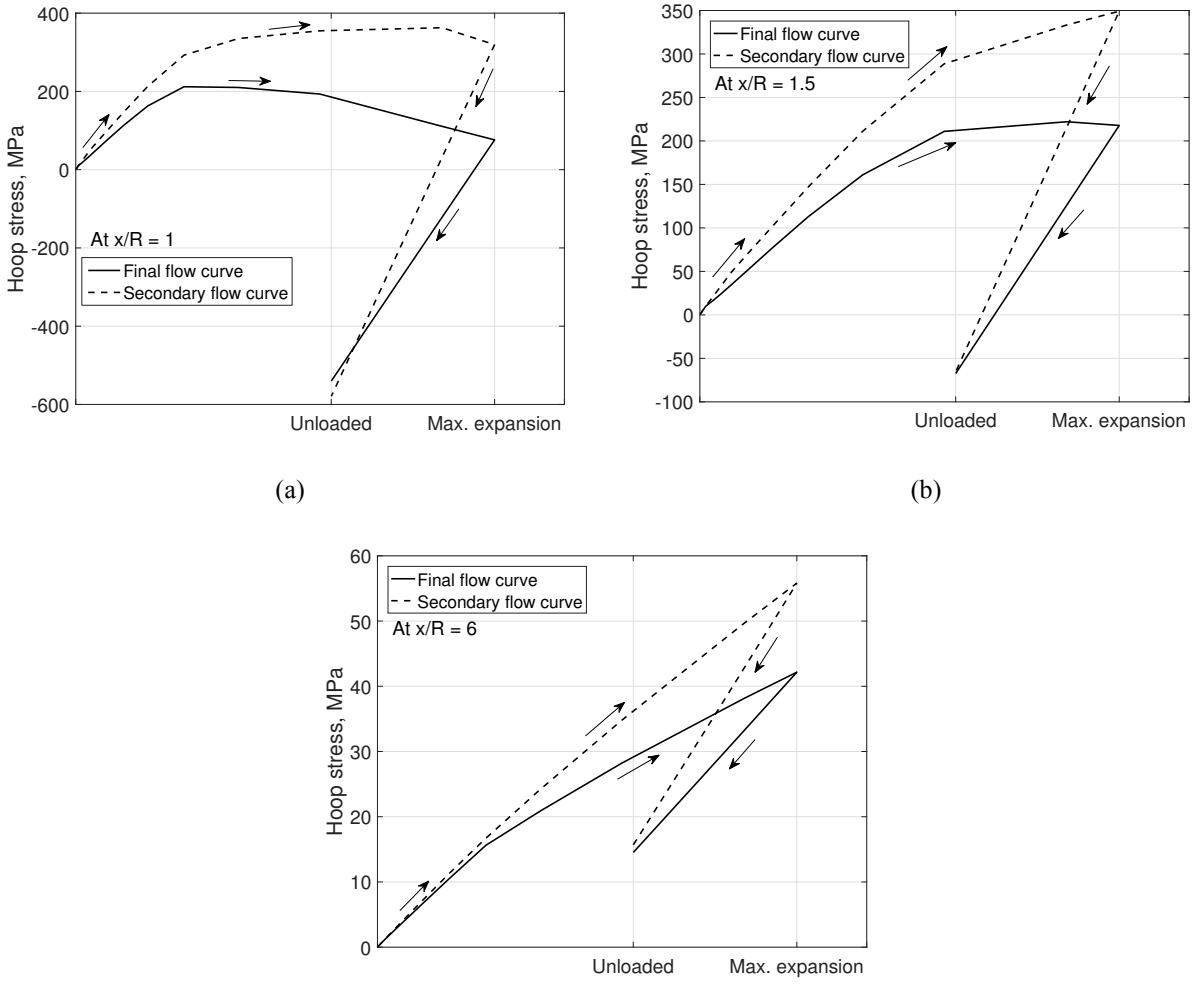

Figure 19 – Hoop stress evolution during the CX process considering the final and secondary flow curves at (a) x/R = 1, (b) x/R = 1.5, (c) x/R = 6